Classification of Dynamic Vibronic Couplings in Vibrational Real-Time Spectra of a Thiophene Derivative by Few-Cycle Pulses[†]

Takayoshi Kobayashi*

Department of Applied Physics and Chemistry and Insititute of Laser Science, University of Electro-communications, Chofugaoka 1-5-1, Chofu, Tokyo, 182-8585 Japan, JST, ICORP, Ultrashort Pulse Laser Project, 4-1-8 Honcho, Kawaguchi, Saitama, Japan, Institute of Laser Engineering, Osaka University, Yamadakami 2-6, Suita 565-0871, Ibaraki 567-0047, Japan, and Department of Electrophysics, National Chiao Tung University, 1001 Ta Hsueh Road, Hsinchu 300,Taiwan

Zhuan Wang

Department of Applied Physics and Chemistry and Institute of Laser Science, University of Electro-communications, Chofugaoka 1-5-1, Chofu, Tokyo, 182-8585 Japan, and JST, ICORP, Ultrashort Pulse Laser Project, 4-1-8 Honcho, Kawaguchi, Saitama, Japan

Tetsuo Otsubo

Department of Applied Chemistry, Hiroshima University, Higashi-Hiroshima 739-8527, Japan

Received: August 22, 2007; In Final Form: September 24, 2007

Pump−probe spectroscopy was performed with a few cycle pulses of 6.7 fs duration. The electronic transition intensity modulation was induced by molecular vibration in a quinoid thiophene molecule in solution. The real-time vibrational features were analyzed in terms of dependence of vibrational amplitude and phase on probe photon energy. The electronic transition probability is modulated by molecular vibration via vibronic coupling. Changes in the spectral shape and intensity of the time-resolved spectrum were studied by tracking characteristic spectral features including the peak frequency and intensity, spectral bandwidth, and band-integrated intensity. From the analysis the modulation mechanisms were classified into two groups: (1) Condon type and (2) non-Condon type. The features of the wave packet motions were also classified into zeroth-order derivatives due to quasi-pure non-Condon type and first- and second-order derivative types due to the displacement of the potential minimum and the potential curvature change associated with the relevant vibronic transition, respectively.

1. Introduction

Several decades ago the development of short-pulse lasers in picosecond regime enabled the study of dynamics of electronic relaxation in various molecular systems.[1−3] Several spectroscopies techniques such as time-resolved absorption and fluorescence spectroscopies have been utilized to study ultrafast dynamics of electronic relaxation.[4−9] The electronic states usually have much broader absorption and emission spectra than vibrational spectra in ordinary molecules. Therefore, it is difficult to assign the transient absorption and emission to some specific species or electronic states with well-defined molecular structure. On the other hand, vibrational spectra can provide the molecular structure information of electronic states. To obtain the information of excited species, such as electronic excited state and intermediate states in the photochemical reaction processes, time-resolved vibrational spectroscopies (TRVS) were utilized. The two most extensively studied TRVS methods are time-resolved Raman scattering spectroscopy and infrared (IR) absorption spectroscopy. They are very useful to acquire vibrational spectra with picosecond to nanosecond time resolu-

tion and have been used quite extensively to study the molecular dynamics in the research filed of TRVS.

Further improvement in femtosecond pulse generation technique has been made to reach the femtosecond time resolution. If we like to follow the gradual change in the molecular structure, then the vibrational frequency of such a system is expected *gradually* to change with a time shorter than 1 ps or several hundred femtoseconds. The situation is encountered when we are tracing a wave packet moving along the potential curve reaching and leaving a transition state between two intermediate states. In such a case, much higher resolution than vibration periods is needed than for the simple case of constant frequency determination. Although, on the other hand, the intermediate state can be studied when the pulse duration of the Raman or IR porbe is shorter than the intermediate lifetime. It is also not possible to obtain the vibrational phase information from the TRVS methods, because both Raman scattering and IR absorption spectroscopies are methodologies not for measuring the amplitude of molecular vibration but for measuring the intensity of the signal without any phase information.

More recent development of an ultrashort pulse laser has enabled us to generate few-cycle pulses in the visible and near-infrared ranges.[10−15] Even subfemtosecond pulses have been obtained by higher harmonic generation in the XUV or soft X-ray regime suitable for the study of inner shell transition of

---

12986 *J. Phys. Chem. A, Vol. 111, No. 50, 2007*

Kobayashi et al.

atoms.[16−18] With femtosecond pulses in the visible range to near IR, real-time vibrational spectroscopy has revealed a wealth of information about vibrational dynamics and coherence in various systems,[19−31] such as in dye molecules,[19,20] polymers,[21−25] metal complexes,[26] and biological substances.[27−30]

In molecular systems and semiconductors, the wave packet is prepared by an ultrashort pump pulse as a coherent excitation of superposition of multivibrational levels and multiphonon states in the ground and/or excited states. Ground-state wave packets can also be created by the stimulated Raman scattering process within pump pulse duration. To obtain the phase of a molecular vibration, we must have some probe to detect the probe-dependent vibrational amplitude ($\Delta I(t)$) on delay time (t) change. The change in electronic transition probability is an excellent tool to obtain instantaneously the vibrational amplitude. It is because the transitions in the visible range take place at much shorter times (in $1-2$ fs depending on the transition energy) than the vibrational periods. Further, more sensitive detectors in the visible and near UV are available to measure the change in transmitted light intensity, which is proportional to $\Delta I(t)$ in the small amplitude change limit. This limit is usually satisfied under ordinary excitation conditions. Typical vibrational periods (frequencies) of aromatic molecules of interest extend from ~ 10 fs (~ 3000 cm^{-1}) to ~ 3 ps (~ 100 cm^{-1}) or even to 10 ps (~ 30 cm^{-1}). Thus, if pulses shorter than vibration periods are used to excite molecules, molecular vibrations can be excited on the ground-state and/or excited-state potential surfaces associated with the electronic transition.

The requirement of the pump pulse needed for the excitation of a molecular coherent vibration mode in the time domain is that the duration of the optical pump pulse must be shorter than the vibration period. Following the short pump pulse excitation, a wave packet is prepared in the form of linear superposition of several vibrational levels of different quantum numbers. Then the wave packet moves on the potential energy surface (PES), and the motion modifies the transition spectra composed of various vibronic transitions between the vibronic levels in the initial and final electronic states. The contributions of the vibrational levels are proportional to the product of the frequency-dependent Franck−Condon factor and the intensity of the pump pulse spectral component corresponding to the vibronic transition energy. Thus the wave packet motion of some vibrational mode can be detected by measuring the time-dependent difference absorbance with another weak probe pulse.

There are several methods to obtain pulses with short enough duration to excite the coherent vibration modes in molecules. Among them, noncollinear phase-matched optical parametric conversion has been attracting great interest as a novel method for ultrashort pulse generation with frequency tunability.[10−14,32] The noncollinear optical parametric amplifiers (NOPA) based on this scheme have been exploited to generate sub-5-fs pulses in the visible spectral range by our group.[10−14] Such ultrashort laser pulses can be applied to study the dynamics utilizing a wave packet modulated electronic transitions through electron-vibration (vibronic) coupling, as outlined above.

Thiophene and its derivatives have been investigated because of their possible optoelectronic applications. Until recently only the type of ordinary thiophene oligomers had been studied and interesting phenomena have been found using such ultrashort pulse lasers.[33−38] Recently, quinoid thiophene oligomers that are geometrical isomers of ordinary thiophene oligomers have been synthesized,[39,40] and it is interesting to study the difference in the vibronic coupling due to the difference in electronic structure.

In the present study, we applied the 6.7 fs real-time spectroscopy to a quinoid thiophene derivative to study the coherent vibrational dynamics of wave packet motion. These wave packet motions were classified into two types according to the mechanisms of the modulation of transient difference absorbance.

2. Experiment

The inset of Figure 1 shows the structure of studied molecule, named as QT2, which is a novel synthesized quinoidal thiophene derivative with two thiophene rings.[39,40] This thiophene substitute has an electron-donating 1,3-dithiol-2-ylidene unit and an electron-withdrawing dicyanomethylene unit at both ends of the long axis of the molecule. The molecule behaves as a push−pull thionoquinoid system with a possible large static dipole moment due to the charge-transfer interaction between the two substituent groups. Solubility in common solvents is introduced by the four methylene butoxy groups attached to the two thiophene rings through pentene rings. In the present study, the concentration of tetrahydrofuran (THF) solution of QT2 was 1.5×10^{-4} mol/dm^3, which gave an optical density of 1.6 at the absorption peak of 690 nm in a 1 mm thick quartz cell.

The stationary absorption and the fluorescence spectra of QT2 shown in Figure 1 were recorded with an absorption spectrometer (Shimadzu, model UV-3101PC) and a fluorophotometer (Hitachi, model F-4500), respectively. The pulsed light source was a NOPA seeded with a white-light continuum.[10−14] The pump source of this NOPA system was a regenerative amplifier (Spectra Physics, model Spitfire) with the following operation parameters: central wavelength, 805 nm; pulse duration, 50 fs; repetition rate, 5 kHz; average output power, 740 mW. The single filament continuum was generated by focusing a small intensity fraction of the amplifier output onto a 1 mm thick sapphire glass.[41−43] The NOPA output pulse was compressed with a pair of chirp mirrors and then with a prism pair, resulting in a Fourier-transform (FT) limited pulse duration of 6.7 fs. The pulse from the NOPA with the spectrum extending from 535 to 725 nm was split into two as the pump and probe pulses with energies of about 45 and 5 nJ, respectively. The pulse duration was slightly longer than the developed sub-5-fs NOPA in our group reported previously[10,13] because of the adjustment of the laser spectrum to optimally excite the QT2 molecule in the longer wavelength range of the NOPA.

In the present study, pump−probe spectroscopy was employed with a combination of polychromator and multichannel lock-in amplifier. The probe pulses were dispersed by the polychromator (300 grooves/mm, 500 nm blazed) and guided to the photodetector by a 128 channel fiber. The spectral resolution of the total system was about 1.5 nm. The transmitted probe spectrum after the sample without the injection of the pump was recorded by averaging 50 000 laser shots. The transmission difference of the probe was accumulated every 3000 laser shots under the excitation conditions by the pump pulse. The pump−probe experiment was performed with a delay time step of 1 fs in the time range $-200-2000$ fs. All experiments were performed at room temperature (293 ± 1 K).

3. Results and Discussion

3.1. Stationary Spectra and Real-Time Difference Absorption Spectrum. The stationary absorption and fluorescence spectra and the stimulated emission spectrum calculated from the latter of the QT2 sample and the laser spectra are shown in Figure 1. The stationary absorption spectrum has two peaks at 650 and 690 nm and a shoulder around 760 nm. The spectrum
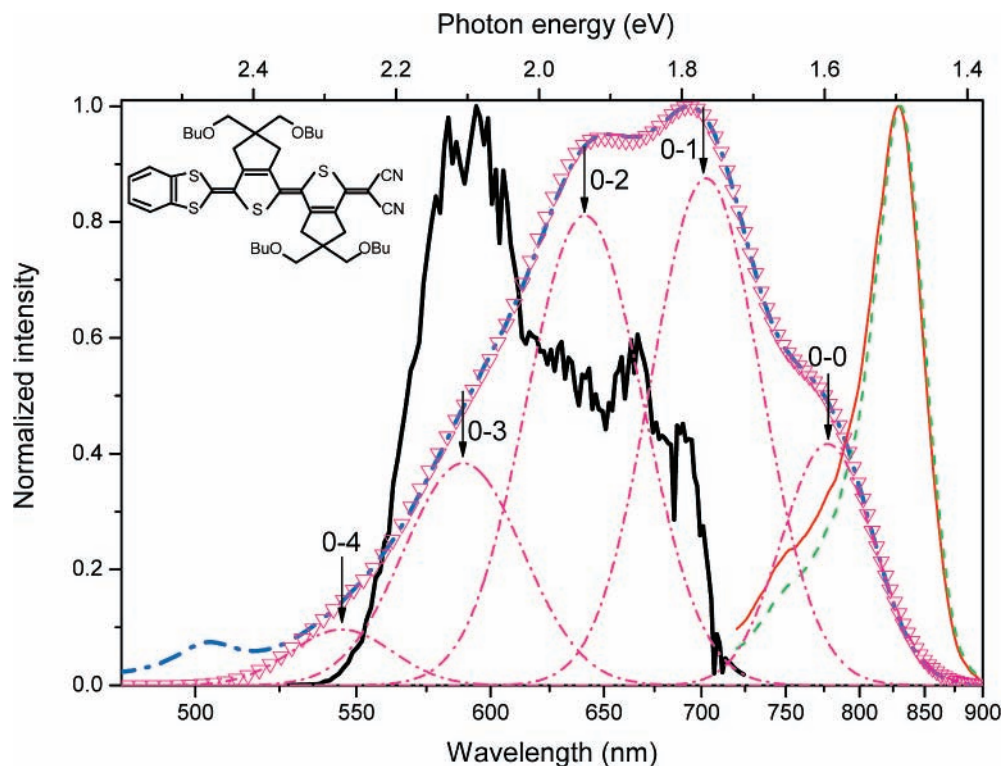
Figure 1. Laser spectrum (thick solid line), stationary absorption (thick dash-dotted line), fluorescence spectrum (thin solid line), and stimulated emission spectrum (dashed line). The inset is the molecular structure used in the present study. The thin dash-dotted lines are the transition bands used in the Huang−Rhys fitting to the stationary absorption and the fitting results are plotted in open triangles. $0 - i$ ($i = 0$, 1, 2, 3, and 4) is the transition from zeroth-vibronic level in the ground state to the ith level in the excited state.

can be fitted with a set of Gaussian bands corresponding to the transition from the vibration level of $v = 0$ in the ground-state to the excited-state vibration level with quantum numbers $v' = 0$, 1, 2, 3, and 4, as shown in Figure 1. The peaks of the Gaussian bands are equally spaced with 0.17 eV (1370 cm^{-1}), which represents the frequency of vibration mode in the excited state. From the distribution of the Gaussian bands, the Huang−Rhys (HR) factor was determined as 1.69. The HR factor is defined as the ratio, $E_{st}/\hbar\omega_v$, between the stabilization energy E_{st} and vibrational energy $\hbar\omega_v$. The stabilization energy is the energy difference between the energy of the Franck−Condon state on the excited-state potential and that of the equilibrium state.

Figure 2a gives several examples of the absorbance change (ΔA) depending on the probe delay time, which are highly modulated and provide the information of the transition probability change due to the wave packet motion on the PES. Figure 2b shows the fast Fourier transform (FFT) of the corresponding real-time traces in the time range from 0 to 2000 fs with respect to a cosine function. The modes appearing in the whole probe wavelength range or relatively broad spectral range are marked with the peak frequencies. There are slight differences among the peak frequencies observed at different wavelengths. This may be due to the limited frequency resolution, estimated to be about ±4 cm^{-1}. It may also be due to the differences in vibration frequencies between the ground state and excited state, both of which couple to the transition at the same wavelength with differing contributions. This is to be addressed later in the paper.

The Raman spectrum of QT2 excited by 514.5 nm line Argon ion laser (NEC, GLG3200) is shown in Figure 2c. Because of a cutoff filter (532 nm) used in the Raman experiment, signals below the 800 cm^{-1} shift could not be detected due to the intense Rayleigh scattering. This indicates that the vibrational real-time spectroscopy has a better detectability than Raman spectroscopy in the case of low-frequency modes. The results in Figure 2b,c

can be compared with each other because Raman active vibrational modes are also active in the real-time spectrum because of the same selection rule controlling the two processes. However, it is still difficult to assign them because the studied sample is a newly synthesized molecue[39,40] and there are not many spectroscopic studies on the system.

Quantum chemical calculation by density functional theory (DFT)[44] was performed to obtain the Raman modes of molecule QT2. According to this theoretical analysis, the vibration assignment was performed in the following.

The vibration modes at 1343, 1420, and 1510 cm^{-1} can be assigned to the twisting, wagging, and scissoring vibration modes of the CH$_2$ group. The mode around 1376 cm^{-1} is due to vibration of CH$_3$ group. The modes at 1172, 1343, and 1510 cm^{-1} can be assigned to modes including the symmetric rotation, breathing, and asymmetric rotation of the benzene ring. The modes around 1376 and 1420 cm^{-1} are the symmetric and asymmetric breathing of the thiophene ring. The modes at 1453 and 1539 cm^{-1} are the symmetric and antisymmetric stretching of five C−C double bond composing the main chain of the molecule. The other modes with low wavenumber are very difficult to identify even by the DFT quantum chemical calculation. They are likely due to one of the ring breathing, torsion, and bending modes of the molecule by comparing with these modes in similar molecules. The details of the assignment and the mechanisms of the activity of the transition probability of the modes are to be discussed elsewhere.[45] In the following section, we will classify the vibration modes according to the vibration phase from the FT results.

3.2. Contributions from the Wave Packet Motion in the Ground and Excited States. The time dependence of the absorbance change due to the wave packet prepared on the ground-state PES (as shown in Figure 3b) can be described with a sine function.[46,47] The time-dependent amplitude modulation
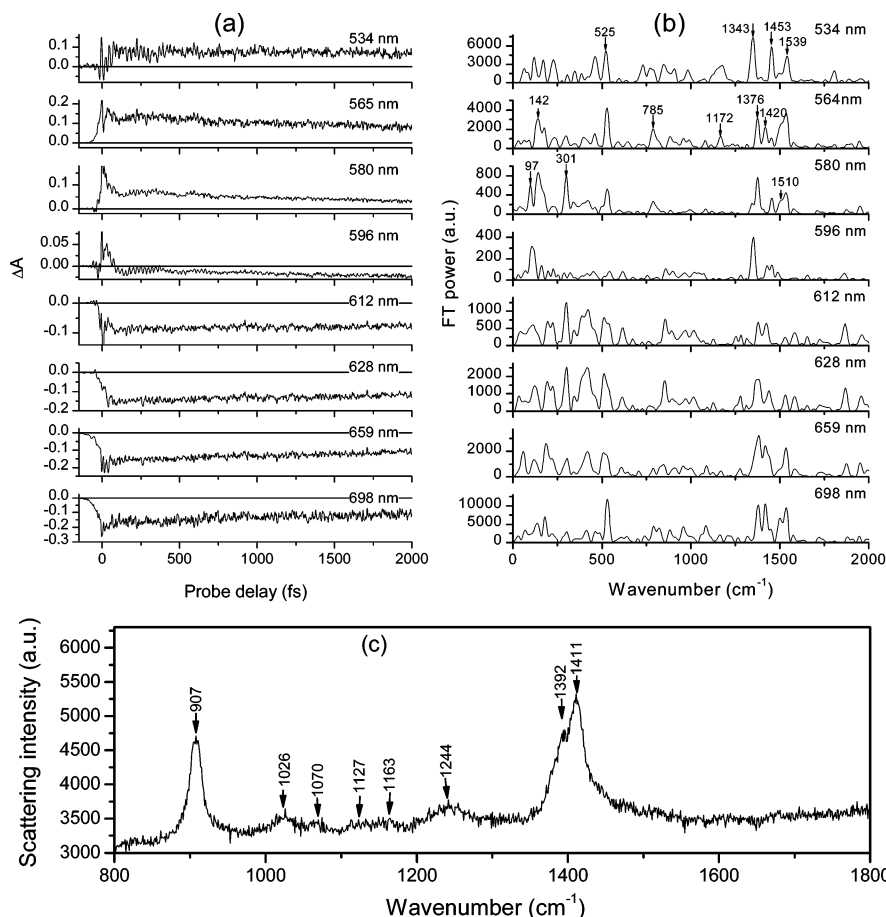
Figure 2. (a) Real-time absorbance change at several probe wavelengths. (b) FT power spectra of the corresponding traces in (a). (c) Raman scattering spectrum of the QT2 molecule with Raman excitation wavelength of 514.5 nm.
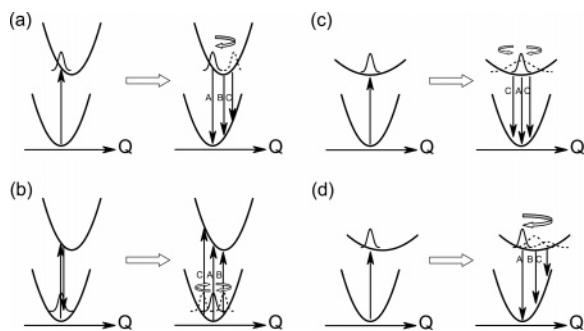

Figure 3. Motions of a wave packet on the (a), (c), and (d) excited-state and (b) ground-state potential energy surface. In the cases of (a), (c), and (d) the phases of the oscillation are 0, $\pi/2$, and π for A, B, and C, respectively. In the case of (b), the phases of the oscillation are 0, $\pi/2$, and $3\pi/2$ for A, B, and C, respectively. Here, Q is the coordinate of the electrons.

induced by the excited-state wave packet motion, as shown in Figure 3a, is given by a cosine function. Hereby, the origin of the wave packet motion will be classified as follows.

The phase of the vibrational modes appearing in Figure 2b is shown in Figure 4 in the spectral range of 540–600 nm (2.30–2.07 eV), which will be used to classify the electronic excited state or the ground state for the wave packet motion. The vibrational mode with phase near $\pm^1/_2\pi$ or $\pm^3/_2\pi$ can be assigned to wave packet motion on the ground state because they correspond to a plus or minus sine function. Those with 0π or $\pm\pi$ phase are due to the excited-state vibration because they are expressed in terms of plus or minus cosine function. For the modes whose phases are different from that of the above-mentioned value are considered to be due to mixed contributions

of the wave packet motions on the ground and excited states. The results of this wave packet motion classification are listed in Table 1.

The mechanism of the dynamic modulation of the electronic transitions associated with the bleaching (BL), induced emission (IE), and induced absorption (IA) processes can be classified into the following two types, which will be discussed later: Condon type and non-Condon type.

3.3. Transient Difference Absorption Spectrum. Figure 5 shows a three-dimensional plot of the time-resolved difference absorption spectrum from 2.32 to 1.72 eV in the probe delay time ranging from 50 to 200 fs, which gives a clear picture of the coherent oscillations. The thick curve on the slope near 2.07 eV ($\sim$600 nm) is the line of null absorbance change, where positive ΔA due to the excited-state absorption (IA) and negative ΔA due to BL and IE cancel each other, resulting in no instantaneous absorbance change at the delay time. The difference absorbance $\Delta A(\omega,t)$ is a function of both probe photon frequency (ω) and probe delay time (t) with respect to the pump pulse peak.

After excitation, the negative $\Delta A(\omega,t)$ were observed in the whole 2 ps probe delay time range for the probe-photon energy E_{prob} lower than 2.10 eV (590 nm). At the probe-photon energies higher than 2.10 eV, the $\Delta A(\omega,t)$ becomes positive because of intensive IA from the electronic excited state. The IE from the excited electronic state seems to contribute very little in this spectral range because the measured fluorescence spectrum is far below, extending from 1.72 to 1.38 eV (720–900 nm). Hence, the negative ΔA observed at photon energy lower than 2.1 eV can be attributed only to the BL of ground-state

Vibronic Couplings in a Thiophene Derivative

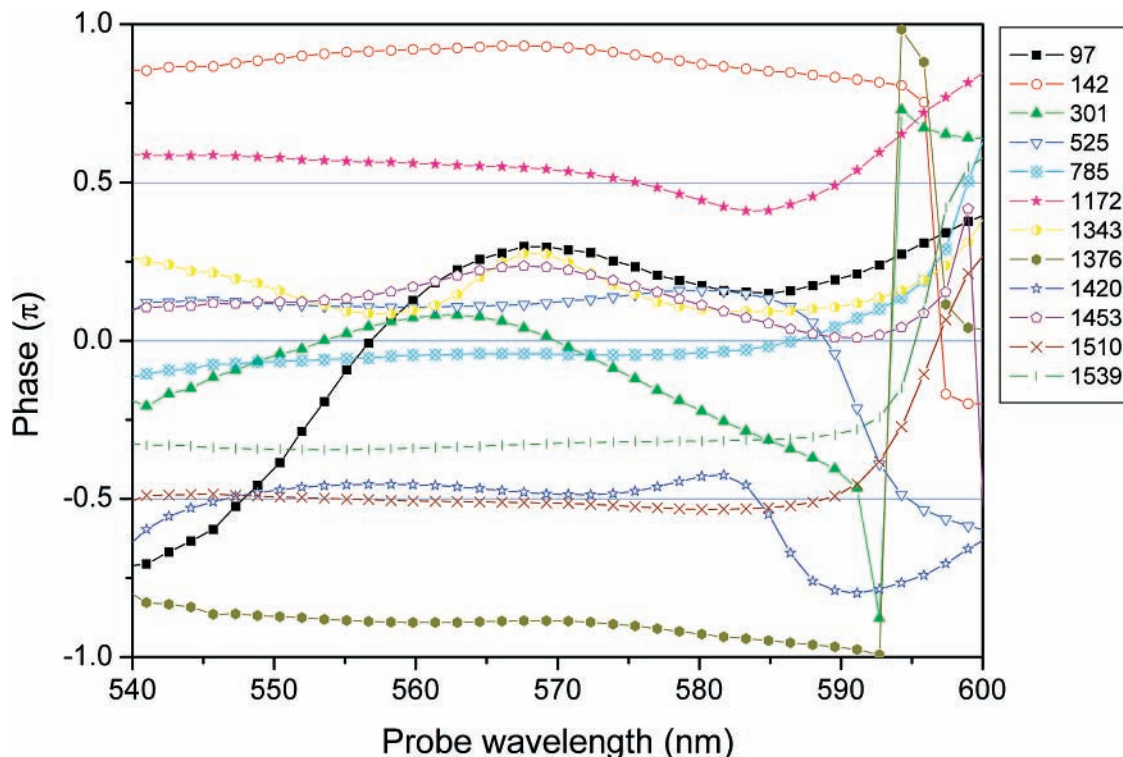*J. Phys. Chem. A, Vol. 111, No. 50, 2007* **12989**

Figure 4. Phases of the vibrational modes appears in the FT results. The legend gives the indication of line shape for different modes.

TABLE 1: Classification of Modes in Terms of Wave Packet Coupling Mechanism[a]

no.	L	P	R	B	P−I	A	R−S	FT−F	FT−P	Wave packet	C 1	C 2	C 3	N−C 0	N−C 1	N−C 2	N−C 3
1		97	101	97				97	$(-3\pi/4-\pi/4)$ (540−570 nm) $\sim\pi/4$ (570−590 nm)	G+E			✓				
2					142	142		142	$\sim\pi$ (540−600 nm)	E				✓			
3	301	293	293		305	305		301	$\sim0\pi$ (540−570 nm)	E	✓						
4					525	525		525	$\sim\pi/8$ (540−600 nm)	E					✓		
5					785	785		785	$\sim0\pi$ (540−600 nm)	E					✓		
6			1176	1176	1172	1168	1163	1172	$\sim\pi/2$ (540−600 nm)	G		✓					
7	1347	1351	1355	1343				1343	$\sim\pi/5$ (540−600 nm)	G+E	✓						
8	1387	1387	1391	1383	1372	1372	1392	1376	$\sim0\pi$ (550−570 nm) $\sim3\pi/4$ (570−590 nm)	E G+E							✓
9	1416	1420		1416	1420	1420	1411	1420	$\sim-\pi/2$ (540−585 nm)	G		✓					
10	1457		1457	1453	1453	1453		1453	$\sim\pi/5$ (540−590 nm)	G+(E)		✓					
11	1510		1510	1510	1510	1510		1510	$\sim-\pi/2$ (540−590 nm)	G						✓	
12		1530			1539	1539		1539	$\sim-2\pi/5$ (540−590 nm)	(G)+E						✓	

[a] L: position of left two-thirds ΔA maximum. P: position of ΔA maximum. R: position of right two-thirds ΔA maximum. B: full width at two-thirds of ΔA maximum. P-I: peak intensity of ΔA. A: band-integrated ΔA area. R-S: Raman scattering of sample in the present study. FT-F: Fourier transform of the real-time ΔA traces. FT-P: phase of Fourier transform of the real-time ΔA traces. Wave packet: energy state (G, ground state; E, excited state). C: Condon type. N-C: non-Condon type (0, 1, 2 indicate the derivative order, and 3 indicates the mixture of first and second derivatives).

absorption. In the range of 2.10−2.30 eV, the spectral shapes of $\Delta A(\omega,t)$ are much simpler than that in the lower photon energy range than 2.10 eV side, as shown in Figure 5. Therefore, the spectral range with positive ΔA is to be discussed in terms of the vibronic coupling in this paper.

In the following discussion, we will introduce the theoretical analysis of the vibration coupling mechanism first and then address the vibration classification afterward.

3.4. Transition Probability Change Due to Wave Packet Motion. The major modes found from the FT power spectra shown in Figure 2b are coupled to the electronic transition corresponding to the excited-state absorption, resulting in the intensity and shape change of the transient different absorption spectra. These properties will be utilized to distinguish the mechanism of the vibronic coupling of each vibration mode.[48]

3.4.1. Condon Type. The electronic transition dipole moment between an initial vibronic state ($\Phi_i(\hat{Q},\hat{q})$) and a final state ($\Phi_f(\hat{Q},\hat{q})$) are expressed as follows, with $\hat{Q}$ and $\hat{q}$ being the coordinates of nucleus and electron,[47] respectively.

$$\langle\Phi_i(\hat{Q},\hat{q})|\hat{\mu}|\Phi_f(\hat{Q},\hat{q})\rangle = \langle\psi_i(\hat{Q},\hat{q})|\langle\chi_i(\hat{Q})|\hat{\mu}|\psi_f(\hat{Q},\hat{q})\rangle\hat{\mu}|\chi_f(\hat{Q})\rangle$$
$$= \langle\psi_i(\hat{Q},\hat{q})|\hat{\mu}|\psi_f(\hat{Q},\hat{q})\rangle\langle\chi_i(\hat{Q})|\chi_f(\hat{Q})\rangle$$
$$= \langle\hat{\mu}\rangle F \quad (1)$$

Here $\hat{\mu}(\hat{q}) = e\hat{q}$ is the dipole operator, $|\chi_a(Q)\rangle$ (a = i, f) is the nuclear wave function, and F is the Franck−Condon factor. The wave functions $|\Phi_i\rangle$ and $|\Phi_f\rangle$ can be the ground state and the excited state, respectively. It is assumed that the transition from the ground state to the excited state is allowed. These two states
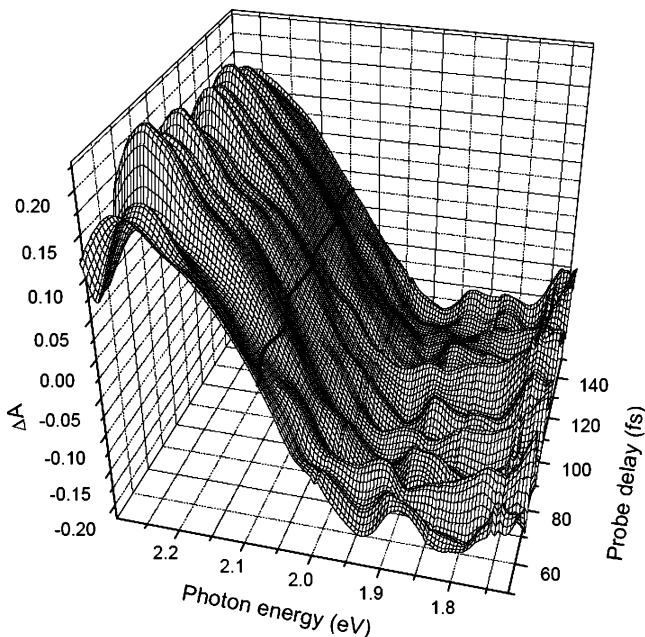
Figure 5. Birds-eye view of the time-resolved difference absorption spectrum of QT2. The line near 2.07 eV (600 nm) represents null absorbance change, where BL and IA cancel each other, resulting in no change in the absorbance.

could also be the lowest excited state and a higher excited state between which dipole transition is allowed.

The change in the transition probability due to molecular vibration is caused by the time-dependent Franck−Condon (FC) factor (F) given below, because $\langle\hat{u}\rangle$ does not depend on the configuration change in the case the Condon approximation is satisfied. The mechanism may be called "time-dependent FC factor" type, but it is called "Condon type" hereafter for simplicity. The expression of the time-dependent FC factor, F, is given by

$$F = \sum_l \sum_m \langle\chi_l(\hat{Q})|x_m(\hat{Q})\rangle = \sum_l \sum_m \langle\chi_l^0(\hat{Q})|\chi_m^0(\hat{Q})\rangle e^{i(l-m)\omega_v t} \quad (2)$$

Here, ω_v is the frequency of relevant molecular vibration due to the vibronic coupling. The prefactor of the sinusoidal function is determined by the Franck−Condon factor and the pump laser spectrum. In many aromatic molecules, displacement of the potential minimum between the ground state and the excited state is not large except for the case of intramolecular excimer type systems. Then Huang−Rhys (HR) factor is not very large as in the case of the present molecule which has the HR value of 1.69. If the HR factor is small due to the small wave packet motion on the potential surfaces of the ground state or the excited state, then it is given by the first derivatives of the corresponding transition spectrum. In this case, the π phase jump at the peak of the corresponding spectrum appears because the transition intensities of higher and lower energy side changes in an anticorrelated manner.

In the above discussion the effect of transition probability modulation was made for a strongly allowed electronic transition dipole moment, in which vibronic coupling does not change substantially the transition dipole moment even though the conformational change due to molecular vibration changes the electronic states. The modulation effect explained above is due to the time-dependent overlap of the nuclear wave packets functions between the initial and the final states. The time-dependent Franck−Condon overlap between can be the linear combination of vibrational wave functions in the ground state

generated by the pump pulse and a set of vibration eigenstates in the excited state or vice versa. Also the components of the pair can be the excited state (initial state of the relevant IA) and the higher excited electronic state (final state).

3.4.2. Non-Condon Type. In the previous subsection, discussion was made for the case of Condon type. In the following we would like to discuss the more general case when it is not satisfied.

The vibronic coupling effect is generally expressed approximately by the expansion of the transition dipole moment operator, $\hat{\mu}(\hat{q},\hat{Q})$, in terms of the displacement of nuclear coordinate from the equilibrium configuration in normal coordinate space. This can be preformed by using the Herzberg− Teller expansion of the ground-state and excited-state wave functions.[49,50] In the present system, we discuss a three-level system composed of three electronic states, S_0, S_1, and S_2, with energies in an increasing order. It is assumed that the vibronic coupling occurs dominantly between S_1 and S_2 states; therefore, the following three wave functions are considered:

$$|S_0(\hat{q},\hat{Q})\rangle = |\psi_0(\hat{q})\rangle|\chi_n^0(\hat{Q})\rangle \quad (3)$$

$$|S_1(\hat{q},\hat{Q})\rangle = \left(|\psi_1(\hat{q})\rangle - \frac{H_{vib}}{\Delta E_{21}}\hat{Q}|\psi_2(\hat{q})\rangle\right)|\chi_m^1(\hat{Q})\rangle \quad (4)$$

$$|S_2(\hat{q},\hat{Q})\rangle = \left(|\psi_2(\hat{q})\rangle - \frac{H_{vib}}{\Delta E_{21}}\hat{Q}|\psi_2(\hat{q})\rangle\right)|\chi_l^2\hat{Q}\rangle \quad (5)$$

In the above equations, $\psi_X(\hat{q})$ and $\chi_k^X(\hat{Q})$ represent wave functions of the electrons and nuclei for the $X = 0$, 1, and 2 for S_0, S_1, and S_2 states, respectively, as a function of the electron and nuclear coordinates, $\hat{q}$ and $\hat{Q}$. In the nuclear wave functions $\chi_k^X(\hat{Q})$, the vibrational quantum number is given by the suffixes $k = n$, l, and m. States S_1 and S_2 are not necessarily the first and second excited states but can be any pair of electronic excited states. The electronic wave function in eq 4, namely, $|\psi_1(\hat{q})\rangle$, consists of two wave functions as follows:

$$|\psi_1(\hat{q})\rangle = |\psi_1^0(\hat{q})\rangle + \alpha|\psi_2(\hat{q})\rangle \quad (6)$$

The second term in (6) originates from the configuration interaction (CI) between S_1 and S_2 bands, the degree of which is described by the coefficient of α. The matrix element of the transition dipole moment from the ground state to the S_1 state is calculated as follows:

$$\langle S_1(q,\hat{Q})|\hat{\mu}(\hat{Q})|S_0(\hat{q},\hat{Q})\rangle =$$
$$\left\langle\chi_m^1(\hat{Q})|(\langle\psi_1(\hat{q})| + \frac{H_{vib}}{\Delta E_{21}}\langle\psi_2(\hat{q})|\hat{Q})\hat{\mu}|\psi_0(\hat{q})\rangle\chi_n^0(\hat{Q})\right\rangle$$

$$= \langle\psi_1(\hat{q})|\hat{\mu}|\psi_0(\hat{q})\rangle\langle\chi_m^1(\hat{Q})|\chi_n^0(\hat{Q})\rangle +$$
$$\alpha\langle\psi_2(\hat{q})|\hat{\mu}|\psi_0(\hat{q})\rangle\langle\chi_m^1(\hat{Q})|\chi_n^0(\hat{Q})\rangle +$$
$$\frac{H_{vib}}{\Delta E_{21}}\langle\psi_2(\hat{q})|\hat{\mu}|\psi_0(\hat{q})\rangle\langle\chi_m^1(\hat{Q})|\hat{Q}|\chi_m^0(\hat{Q})\rangle$$

$$= F_1 + F_2 + F_3 \quad (7)$$

$$F_1 \equiv \mu_{10}^0\langle\chi_m^1|\chi_n^0\rangle \quad (8)$$

$$F_2 \equiv \alpha\mu_{20}\langle\chi_m^1|\chi_n^0\rangle \quad (9)$$

$$F_3 \equiv \beta\mu_{20}Q_{mn} \quad (10)$$

Here, $\mu_{10}^0 = \langle\psi_1^0|\hat{\mu}|\psi_0\rangle$, $\mu_{20} = \langle\psi_2|\hat{\mu}|\psi_0\rangle$, $\beta = H_{vib}/\Delta E_{21}$, and $Q_{mn} = \langle\chi_m^1|\hat{Q}|\chi_n^0\rangle$. F_1 is the term corresponding to the ordinary

Vibronic Couplings in a Thiophene Derivative

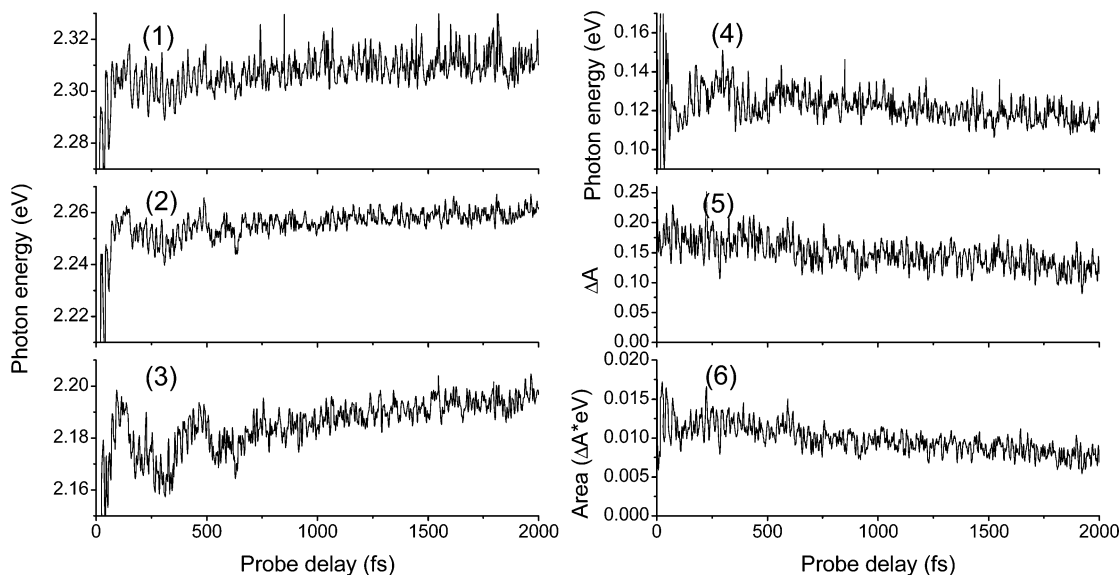*J. Phys. Chem. A, Vol. 111, No. 50, 2007* **12991**

Figure 6. Position-tracking results as a function of probe-delay time; (1) two-thirds of ΔA maximum at the high-photon-energy side; (2) the ΔA maximum; (3) the two-thirds of ΔA maximum at the low-photon-energy side. (4) Full bandwidth of the ΔA transient spectra at the two-thirds of the maximum. (5) ΔA intensities at the maximums. (6) Integrated area of the ΔA transient spectra in the photon energy range defined by the two-thirds of the maximum.

Franck−Condon factor without non-Condon effect. F_2 is a term for static intensity borrowing (exchange) by the electron correlation mechanism. However, concerning the modulation of the transition probability induced by molecular vibration it gives the same result as F_1. Finally, F_3 is the term of dynamic intensity borrowing (DIB) by the vibronic coupling.[51] DIB is the process of inter-electronic-state exchange of electronic transition probability through vibration observed during the real-time molecular vibration as discussed in our previous paper.[51]

The corresponding vibration wavenumber to the present experimental temperature of 293 K was estimated to be 200 cm^{-1} from $\hbar\omega_{vib}/k$, where $\hbar$, ω_{vib}, and k are the reduced Planck constant, relevant vibrational frequency, and the Boltzmann constant, respectively. For modes with frequency higher than 600 cm^{-1}, the population on the higher vibration level is more than 20 times smaller. Therefore, the initial population on the vibrational levels with vibrational quantum number larger than zero can be neglected. Then $|\chi_n^0\rangle$ is set to be $|\chi_0^0\rangle$. However, for modes with wavenumber lower than 600 cm^{-1}, the contribution is partially from the vibration level with larger quantum numbers than zero.

The above discussion given in the last paragraph is about the excitation process. Now we proceed to the problem of the probing process. The terms of F_1 and F_2 are proportional to the time-dependent Franck−Condon factor $\langle\chi_m^1|\chi_n^1\rangle$. The time-integrated Franck−Condon factor can be given by the following population distribution when the vibrational quantum number of the vibrational level in the ground state is $m = 0$ and the pump laser is much shorter than the probe duration.

$$\langle\chi_m^1|\chi_0^0\rangle = \sum_l \frac{\bar{l}^l}{(l_1^1)^{\frac{1}{2}}} e^{-\bar{l}} \equiv P_{\bar{l}} \qquad (10)$$

Where $\bar{l}$ is the averaged vibrational quantum number after photoexcitation and corresponds to the Huang−Rhys factor introduced earlier. The term F_3 is proportional to $\langle\chi_m^1|\hat{Q}|\chi_n^1\rangle$. This can be represented by

$$\langle\chi_m^1|\hat{Q}|\chi_n^1\rangle = P_{\bar{l}+1} \qquad (11)$$

The result means that the profile of the probe spectral dependence of Condon type and non-Condon type are similar when the vibrational quantum number of the initial electronic state is zero. F_1 and F_2 are activated when the potential minimum is shifted upon photoexcitation from the ground state to the excited state or when the relevant molecular vibration frequency of the ground state and that of the excited state is substantially different without displacement of the minimum. In the former case the spectral change will be the first derivative of the relevant transition spectrum namely, absorption BL, IE, or IA spectra. In the latter case the wave packet motion is not a displacing motion of the weight of mass of the wave packet as shown in Figure 3c,d. Therefore the spectral change is given approximately by the second derivative of the relevant transition (BL, IA, and/or IE) spectrum.

Then the mechanism of the transition probability modulation can be classified into two. The first one is the case when only F_1 and F_2 are contributing because of the satisfied Condon approximation. This is the case of Condon type as discussed in the previous subsection. Second is the case where the Condon approximation is not satisfied and the non-Condon type effect is the main origin of the modulation intensity. Both types can be classified into subgroups of (a) potential displacement type, (b) curvature change type, and (c) mixed type, as shown schematically in Figure 3a−d, respectively.

3.5. Analysis of Transient Difference Absorption Spectra in the Probe Energy Range Higher Than 2.10 eV. According to the above discussion, the dynamics of the probe delay time (t)-dependent difference absorption spectrum $\Delta A(\omega,t)$ caused by the wave packet motion in this range was analyzed by employing the tracking method developed in our previous paper.[52] Characteristic spectral points of the transition intensity peak, spectral bandwidth, peak intensity, and band-integrated intensity were utilized to study the wave packet motion. The analysis procedure is described as follows:

(1) determination of the photon energy, $P(t)$, of a peak of $\Delta A(\omega,t)$ and the ΔA value, $A_P(t)$, at this peak by fitting the observed spectrum $\Delta A(\omega,t)$ to a parabolic curve within a 100 meV range next to the peak;
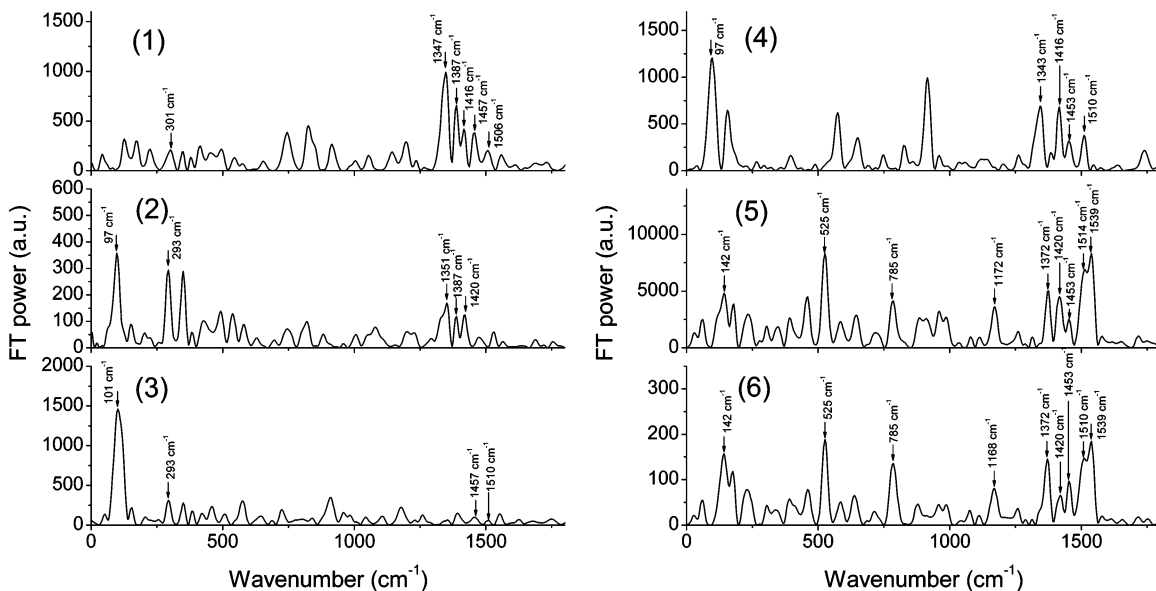
Figure 7. FFT power spectra of the six traces shown in Figure 6.
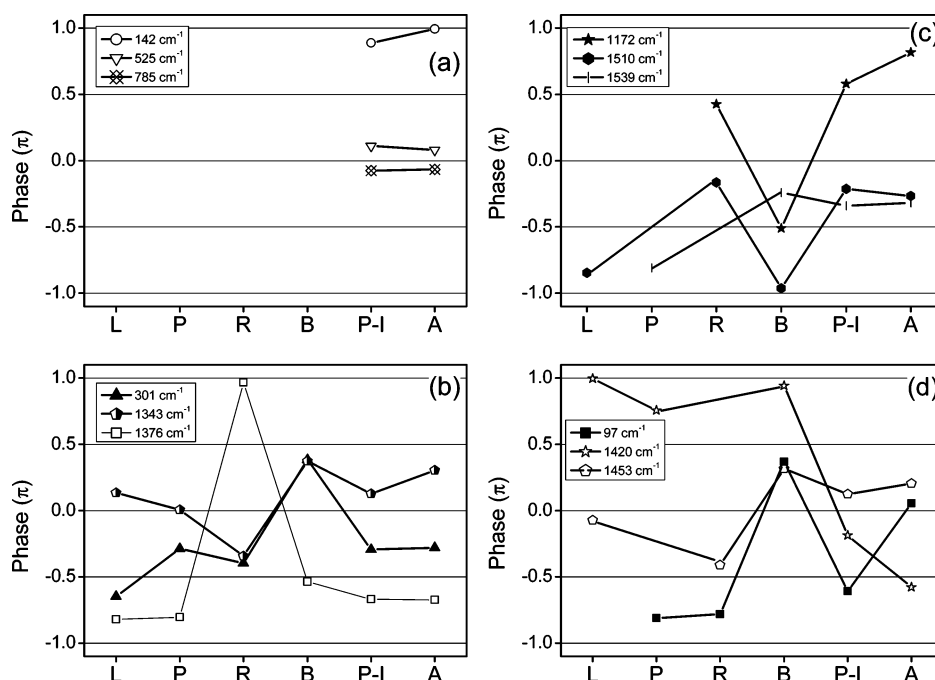

Figure 8. Phase of modes appeared in Figure 7. (a)−(d) depict classification of the modes according to the phase relationship to the zeroth-order, first-order, and second-order effects and the first and second mixed effect. The legend gives an indicator of the line shape of the different modes. The meanings of the characters at the bottom are given in the caption of Table 1.

(2) determination of the photon energies of the two-thirds of ΔA peak at both sides of the ΔA band ($L(t)$, lower energy side; $H(t)$, higher energy side) and the full width at the two-thirds of peak ΔA, $B(t)$; the positions of $L(t)$, $H(t)$, and $B(t)$ were determined by interpolation from the data points of the observed difference spectra;

(3) calculation of the integrated signal intensity, $\Delta A^{I}(t) = \int \Delta A(\omega,t)\,d\omega$, in the probe-photon energy range determined by the photon energies at two-thirds of the ΔA maximum.

The time traces obtained by the above-mentioned analysis are shown in Figure 6. All of them are highly modulated, which indicates that the wave packet motion is highly coupled to the electronic transition, resulting in the change in the transition energy and intensity. The modulation frequencies were determined by the Fourier transform, the results of which are shown

in Figure 7, and they were also found in the FT of the traces of the difference absorbance as shown in Figure 2b.

In this range, the absorption BL is expected to be small, as can be seen from the weak stationary absorption intensity shown in Figure 1. Therefore we will neglect the small BL contribution in the following analysis and discussion.

On the other hand, the high-energy side of the IA extends beyond the available energy range of probe photon from the NOPA. Therefore, the two spectral points whose photon energies are the two-thirds of the ΔA maximum on both sides were used to study the bandwidth of the induced absorption due to the excited state. We used the integrated signal $\int \Delta A(\omega)\,d\omega$ in the photon energy range between the two spectral points with the two-thirds maximum ΔA to estimate the total IA transition probability. It corresponds to the intensity of transition from

Vibronic Couplings in a Thiophene Derivative

J. Phys. Chem. A, Vol. 111, No. 50, 2007 **12993**

the lowest excited electronic state to higher excited state(s). The wave packet on the excited state is composed of the linear superposition of several vibrational levels with different quantum numbers.

3.6. Classification of the Wave Packet Motion. From the theoretical discussion in the previous subsection on the Condon type and non-Condon type, the results in Figures 7 and 8 are used to classify the vibronic coupling mechanism.

First of all, the integrated difference absorbance ($\Delta A^I(t)$) is to be considered to distinguish the Condon type and non-Condon type. In the ideal case, the integrated difference absorbance does not change for the Condon type. However, in real molecular systems, it becomes complicated because of the mixed contribution of several vibrational modes due to deviation from the ideal assumption. Here, the modes shown in Figure 7-(6) were divided to three levels (weak, medium, and strong) according to the vibrational intensity. The modes with frequencies of 142, 525, 785, 1376, 1510, and 1539 cm^{-1} giving strong vibration amplitude were classified as non-Condon type. The other modes were assigned to the Condon type.

Second, the time-resolved spectral change induced by the coupling will be taken into consideration, which will be used to classify the Condon and non-Condon types into subgroups of (a) potential minimum displacement type, (b) potential curvature change type, and (c) mixed type. In these three cases, the time-resolved spectra behave as the spectral shift, spectral breathing, and the mixed spectral change, respectively. Figure 8 shows the phases of the modes that appeared in Figure 7, The explanation of the symbols L, P, R, B, P-I, and A given at the bottom of Figure 8, which is also given in the caption of Table 1, is as follows: L, position of left two-thirds ΔA maximum; P, position of ΔA maximum; R, position of right two-thirds ΔA maximum; B, full width at two-thirds of ΔA maximum; P-I, peak intensity of ΔA; A, band-integrated ΔA area. The phases in Figure 8 were utilized to characterize the spectral change and perform the classification, which is described in the following.

(1) Among the modes shown in Table 1, there are three modes, 142, 525, and 785 cm^{-1}, that do not show spectral change, as shown in Figure 8a, but only the in-phase peak intensity and integrated intensity change. This kind of feature was classified into the zeroth-order derivative due to pure non-Condon type.

(2) The in-phase motion of all of L, P, and R positions indicates the spectral shift, as shown in Figure 8b for modes 301 and 1343 cm^{-1}, and the probe photon energy dependence of vibrational amplitude is approximately given by a first-order derivative of the transition spectrum due to the potential minimum displacement.

(3) The antiphase behavior of L and R gives a spectral breathing, as shown in Figure 8c for mode 1510 cm^{-1}, and the vibrational amplitude is approximately given by second-order derivative of the transient spectrum due to the curvature change. For modes of 1172 and 1539 cm^{-1}, they are classified into the breathing type because of the obvious vibration feature of B in the case of no antiphase motion of L and R.

(4) An even more complicated condition could be expressed by the combination of (2) and (3) and is assigned to the mixed-type model of potential minimum displacement and curvature change.

4. Conclusion

With a 6.7 fs pulse, the real-time vibrational features were studied for a quinoid thiophene through the modulation of

transition probability. Spectral shape and intensity changes were studied by tracking characteristic spectral points of transition intensity peak, spectral bandwidth, peak intensity, and band-integrated intensity. From the analysis, the transition probability modulation behaviors were classified into two groups, i.e., (1) Condon type and (2) non-Condon type. Both groups were classified into subgroups of (a) potential displacement type, (b) curvature change type, and (c) mixed type. From this method, the mechanism of vibronic coupling in molecules can well be understood in terms of features of the changes in the potential curves of the electronic transition states associated with transition.

References and Notes

(1) Shank, C. V., Ippen, E. P., Shapiro, S. L., Eds. *Springer Series in Chemical Physics 4: Picosecond Phenomena*; Spinger Press: Berlin, 1978.

(2) Hochstrasser, R. M., Kaiser, W., Shank, C. V., Eds. *Springer Series in Chemical Physics 14: Picosecond Phenomena II*; Spinger Press: Berlin, 1980.

(3) Eisenthal, K. B., Hochstrasse, R. M. r., Kaiser, W., Laubereau, A., Eds. *Springer Series in Chemical Physics 23: Picosecond Phenomena III*; Spinger Press: Berlin, 1982.

(4) Laubereau, A., Stockburger, M., Eds. *Time-Resolved Vibrational Spectroscopy*; Springer-Verlag Press: Berlin, 1985.

(5) Schreiber, E., Ed. *Springer Tracts in Morden Physics 143: Femtosecond Real-Time Spectroscopy of Small Molecules and Clusters*; Springer Press: Berlin, 1998.

(6) De Schryver, F. C., De Feyter, S., Schwertzer, G., Eds. *Femtochemistry*; Wiley-VCH Press: New York, 2001.

(7) Martin, M. M., Hynes, J. T., Eds. *Femtochemistry and Femtobiology, Ultrafast events in molecular science*; Elsevier Press: Amsterdam, 2004.

(8) Hannaford, P., Ed. *Femtosecond Laser Spectroscopy*; Springer Press: Berlin, 2005.

(9) Castleman, A. W., Jr., Kimble, M. L., Eds. *Femtochemistry VII, Fundamen- tal Ultrafast Processes in Chemistry, Physics, and Biology*; Elsevier Press: Amsterdam, 2006.

(10) Shirakawa, A.; Sakane, I.; Kobayashi, T. *Opt. Lett.* **1998**, *23*, 1292.

(11) Shirakawa, A.; Sakane, I.; Takasaka, M.; Kobayashi, T. *Appl. Phys. Lett.* **1999**, *74*, 2268.

(12) Kobayashi, T.; Shirakawa, A. *Appl. Phys. B* **2000**, *70*, S239.

(13) Baltuska, A.; Kobayashi, T. *Appl. Phys. B* **2002**, *75*, 427.

(14) Baltuska, A.; Fuji, T.; Kobayashi, T. *Opt. Lett.* **2002** *27* 306.

(15) Yamashita, M.; Yamane, K.; Morita, R. *IEEE J. Select. Top. Quantum Electron.* **2006**, *12*, 213.

(16) Baltuska, A.; Udem, Th.; Uiberacker, M.; Hentschel, M.; Gouliel-makis, E.; Gohle, Ch.; Holzwarth, R.; Yakovlev, V. S.; Scrinzi, A.; Hansch, T. W.; Krausz, F. *Nature* **2003**, *421*, 611.

(17) Tsakiris, G. D.; Eidmann, K.; Meyer-ter-Vehn, J.; Krausz, F. *New J. Phys.* **2006**, *8*, 19.

(18) Drescher, M.; Hentschel, M.; Kienberger, M.; Uniberacker, M.; Yakovlev Scrinzi, V. A.; Westerwalbesloh, Th.; Kleineberg, U.; Heinzmann, U.; Krausz, F. *Nature* **2002**, *419*, 803.

(19) Fragnito, H. L.; Bigot, J. Y.; Becker, P. C.; Shank, C. V. *Chem. Phys. Lett.* **1989**, *160*, 101.

(20) Pollard, W. T.; Dexheimer, S. L.; Wang, Q.; Peteanu, L. A.; Shank, C. V.; Mathies, R. A. *J. Phys. Chem.* **1992**, *96*, 6147.

(21) Adachi, S.; Kobryanskii, V. M.; Kobayashi, T. *Phys. Rev. Lett.* **2002**, *89*, 27401.

(22) Ishii, N.; Tokunaga, E.; Adachi, S.; Kimura, T.; Matsuda, H.; Kobayashi, T. *Phys. Rev. A* **2004**, *70*, 023811.

(23) Cerullo, G.; Lanzani, G.; Muccini, M.; Taliani, C.; Silvestri, S. D. *Phys. Rev. Lett.* **1999**, *83*, 231.

(24) Lanzani, G.; Cerullo, G.; Stagira, S.; Zavelani-Rossi, M.; De Silvestri, S. *Synth. Met.* **2001**, *119*, 491.

(25) Kobayashi, T.; Shirakawa, A. *Chem. Phys. Lett.* **2000**, *321*, 385.

(26) Sugita, A.; Saito, T.; Kano, H.; Yamashita, M.; Kobayashi, T. *Phys. Rev. Lett.* **2001**, *86*, 2158.

(27) Kobayashi, T.; Saito, T.; Ohtani, H. *Nature* **2001**, *414*, 531.

Kobayashi et al.

(28) Vos, M. H.; Rappaport, F.; Lambry, J. C.; Breton, J.; Martin, J. L. *Nature* **1993**, *363*, 320.

(29) Chachisvilis, M.; Sundstrom, V. *Chem. Phys. Lett.* **1996**, *261*, 165.

(30) Monshouwer, R.; Baltuska, A.; Mourik, F. V.; Grondelle, R. V. *J. Phys. Chem. A* **1998**, *102*, 4360.

(31) Rosker, M. J.; Wise, F. W.; Tang, C. L. *Phys. Rev. Lett.* **1986**, *57*, 321.

(32) Baum, P.; Lochbrunner, S.; Riedle, E. *Appl. Phys. B* **2004**, *79*, 1027.

(33) Yang, A.; Kuroda, M.; Shiraishi, Y.; Kobayashi, T. *J. Chem. Phys.* **1998**, *109*, 8442.

(34) Sugita, A.; Shiraishi, Y.; Kobayashi, T. *Chem. Phys. Lett.* **1998**, *296*, 365.

(35) Ozawa, A.; Takimiya, K.; Otsubo, T.; Kobayashi, T. *Chem. Phys. Lett.* **2005**, *409*, 224.

(36) Kobayashi, T.; Wang, H.; Wang, Z.; Otsubo, T. *Chem. Phys. Lett.* **2006**, *426*, 105.

(37) Kobayashi, T.; Wang, H.; Wang, Z.; Otsubo, T. *J. Chem. Phys.* **2006**, *125*, 044103.

(38) Wang, Z.; Otsubo, T.; Kobayashi, T. *Chem. Phys. Lett.* **2006**, *430*, 45.

(39) Takahashi, T.; Takimiya, K.; Otsubo, T.; Aso Y. *Org. Lett.* **2005**, *7*, 4313.

(40) Takahashi, T.; Matsuoka, K.; Takimiya, K.; Otsubo, T.; Aso Y. *J. Am. Chem. Soc.* **2005**, *27*, 8928.

(41) Reed, M. K.; Steiner-Shepard, M. K.; Negus, D. K. *Opt. Lett.* **1994**, *19*, 1855.

(42) Yakovlev, V. V.; Kohler, B.; Wilson, K. R. *Opt. Lett.* **1994**, *19*, 2000.

(43) Reed, M. K.; Steiner-Shepard, M. K.; Armas, M. S.; Negus, D. K. *J. Opt. Soc. Am. B* **1994**, *19*, 1855.

(44) Frisch, M. J.; Trucks, G. W.; Schlegel, H. B.; Scuseria, G. E.; Robb, M. A.; Cheeseman, J. R.; Montgomery, J. A.; Vreven, T., Jr.; Kudin, K. N.; Burant, J. C.; Millam, J. M.; Iyengar, S. S.; Tomasi, J.; Barone, V.; Mennucci, B.; Cossi, M.; Scalmani, G.; Rega, N.; Petersson, G. A.; Nakatsuji, H.; Hada, M.; Ehara, M.; Toyota, K.; Fukuda, R.; Hasegawa, J.; Ishida, M.; Nakajima, T.; Honda, Y.; Kitao, O.; Nakai, H.; Klene, M.; Li, X.; Knox, J. E.; Hratchian, H. P.; Cross, J. B.; Bakken, V.; Adamo, C.; Jaramillo, J.; Gomperts, R.; Stratmann, R. E.; Yazyev, O.; Austin, A. J.; Cammi, R.; Pomelli, C.; Ochterski, J. W.; Ayala, P. Y.; Morokuma, K.; Voth, G. A.; Salvador, P.; Dannenberg, J. J.; Zakrzewski, V. G.; Dapprich, S.; Daniels, A. D.; Strain, M. C.; Farkas, O.; Malick, D. K.; Rabuck, A. D.; Raghavachari, K.; Foresman, J. B.; Ortiz, J. V.; Cui, Q.; Baboul, A. G.; Clifford, S.; Cioslowski, J.; Stefanov, B. B.; Liu, G.; Liashenko, A.; Piskorz, P.; Komaromi, I.; Martin, R. L.; Fox, D. J.; Keith, T.; Al-Laham, M. A.; Peng, C. Y.; Nanayakkara, A.; Challacombe, M.; Gill, P. M. W.; Johnson, B.; Chen, W.; Wong, M. W.; Gonzalez, C.; Pople, J. A. *Gaussian 03*, revision D.02; Gaussian, Inc.: Wallingford, CT, 2004.

(45) Kobayashi, T.; Wang, Z.; Iwakura, I. Submitted to *Phys. Rev. Lett.*

(46) Kumar, A. T. N.; Rosca, F.; Widom, A.; Champion, P. M. *J Chem. Phys.* **2001**, *114*, 701.

(47) Kumar, A. T. N.; Rosca, F.; Widom, A.; Champion, P. M. *J Chem. Phys.* **2001**, *114*, 6795.

(48) Lin, S. H.; Eyring, H. *Proc. Natl. Acad. Sci. U.S.A.* **1974**, *71*, 3145.

(49) Lin, S. H.; Eyring, H. *Proc. Natl. Acad. Sci. U.S.A.* **1974**, *71*, 3802.

(50) Kano, H.; Saito, T.; Kobayashi, T. *J. Phys. Chem. A* **2002**, *106*, 3445.

(51) Kano, H.; Saito, T.; Kobayashi, T. *J. Phys. Chem. B* **2001**, *105*, 413.

(52) Yuasa, Y.; Ikuta, M.; Kobayashi, T. *Phys. Rev. B* **2005**, *72*, 134302.